ISME

The Iranian Journal of Mechanical Engineering Transactions of ISME
Journal homepage: https://jmee.isme.ir/
Vol. 27, No. 1, 2026

Research Paper

DOI: 10.30506/jmee.2025.2052983.1370

Perturbation technique in thermoelastic analysis of thick cylinders under various boundary conditions using shear deformation and temperature theories

Moslem Mahmoodi[1]
PhD Student

Mehdi Ghannad[2]
Professor

Mohammad Zamani Nejad[3]
Associate Professor

This paper analyzes the thermoelasticity of the thick-walled cylindrical shell under pressure and thermal loading on the inner surface of the shell. First-order shear deformation and First-order temperature theories are used to determine the displacement and temperature fields, respectively, which include displacement and temperature changes along the length and thickness of the shell. The system's governing equations and boundary conditions have been derived utilizing the energy method. The system of governing differential equations was solved using the analytical process of matched asymptotic method of perturbations technique. The mechanical and temperature behavior of the cylindrical shell has been analyzed by solving the equations and obtaining the displacement and temperature parameters. The analytical solution was then compared with the numerical solution, showing a substantial similarity in behavior. Moreover, the effectiveness of the proposed method in addressing axisymmetric cylindrical shells under various boundary conditions and thermo-mechanical loading is demonstrated. Examining the shell's mechanical and thermal behavior reveals that shear stress changes significantly near the boundaries, and both displacement and temperature fields are influenced by the cylindrical shell's length.

Keywords: Thermoelasticity, Thick cylinders, Shear deformation theory, Perturbation technique, Matched asymptotic method (MAM).

[1]PhD Student, Faculty of Mechanical Engineering, Shahrood University of Technology, Shahrood, Iran
[2]Professor, Faculty of Mechanical Engineering, Shahrood University of Technology, Shahrood, Iran
[3]Associate Professor, Faculty of Mechanical Engineering, Yasouj University, Yasouj, Iran

1. Introduction

In general, Shells are curved structures placed in the highest order of evolution of structures in terms of behavioral quality and resistance to forces and anchors. It is vital to analyze them according to behavioral desirability. The available analytical approximate methods for the analysis of shells are based on the assumptions that form the theory of shells. Among the types of shells, cylindrical shells are of special importance due to their many applications. The study of the behavior of such shells has been the focus of scientists since the not-so-distant past and continues. Researchers have been pursuing changes in the geometry and material of the shells to increase their resistance against various mechanical and thermal stresses.

In recent years, with the increasing growth of various industries, including aerospace industries, turbines, reactors, etc., the use of axially symmetric shells has increased widely. Thermal stresses also affect many structures and mechanical parts used in industries and bearing mechanical loads. Therefore, due to their wide application, the analysis of the thermal-mechanical response of these shells against different loadings and boundary conditions has been an essential part of the researchers' recent research. Mathematical methods are considered compelling tools for solving engineering problems, especially thermoelasticity problems, due to the presented solution's high accuracy and generality.

The analytical solution method solves an equation in the entire domain of the problem by using mathematical principles and without introducing approximation. In contrast, the numerical solution method is a technique that solves problems using approximately a limited number of mathematical sentences. Therefore, the result of the numerical solution will usually be only one answer, while the analytical solution answers a complete set of problems. In other words, the numerical method must be recalculated for each set of parameters. Still, in most cases, the analytical method enables the development and generalization of answers in different conditions.

Ghannad et al. presented the general solution of thick-walled and isotropic truncated conical shells based on the first-order shear deformation theory (FSDT) with the help of matched asymptotic method (MAM) [1]. Ghannad and Nejad derived the governing equations for homogeneous and isotropic thick-walled cylinders based on shear deformation theory. They solved the resulting linear inhomogeneous differential equation system with the help of eigenvalue problems (EVP) [2]. Ghannad and Nejad presented an analysis of axisymmetric heterogeneous thick-walled cylinders under pressure on the internal and external surfaces based on the first-order shear deformation theory, then compared the results obtained from plane elasticity theory (PET) and the finite element method (FEM) [3]. Using the first-order shear deformation theory and matched asymptotic method of perturbation technique, An analytical solution for the deformation and stresses of a cylindrical shell with varying thickness, made of functionally graded materials (FGMs) and under internal pressure, was provided by Ghannad et al. [4]. Using the finite element method, Shojaeefard and Najibi analyzed the hollow, thick-walled cylinder under transient thermal loading [5]. Jiang and Dai presented an analytical solution for two-dimensional and three-dimensional problems of steady and transient heat transfer of a double-layer plate with a heat source. They solved the governing equations in the steady state using the Poisson's method and in the transient state by separating variables. They also investigated the effect of heat source and time on temperature distribution [6]. Ghannad and Parhizkar obtained the thermoelasticity equations of thick-walled cylinders using the first-order shear deformation theory and eigenvalue problems. Then, they compared the results in various boundary conditions [7]. Jabbari et al. presented the stress distribution of FGM cylindrical shells with different thicknesses under thermomechanical loading. To describe the nature of the thermal-elastic behavior of cylindrical shells, they used the higher-order shear deformation theory (HSDT). They evaluated the problem using the semi-analytical multilayer method (MLM) [8]. Khoshgoftar et al. used the shear deformation theory and potential energy method to derive the equations for a functionally graded material cylinder with variable thickness under non-

uniform pressure for thermoelastic analysis. They solved the resulting non-homogeneous cylinder equations using the perturbation technique [9]. Arefi et al. used the first-order shear deformation theory and two-dimensional thermoelasticity to derive the equations for a FGM cylindrical pressure vessel with axially variable thermal and mechanical loads. The four differential equations of the system were solved using the eigenvalue problem methods for different axial variable loading patterns. [10]. Ghannad and Parhizkar have derived the governing equations for an axially symmetric cylinder under pressure and heat flux using the shear deformation theory and first-order temperature theory. Then, they solved the resulting equations using the eigenvalue problem. Then, they investigated the impact of varying pressure and heat flux on the displacements and stresses of the cylinder [11]. Using first-order shear deformation theory, Vaziri and Ghannad derived the governing equations for axisymmetric thick-walled cylinders under transient thermal loading in the general state [12]. Mehditabar et al. analyzed the three-dimensional asymmetric problem of the conical shell with FG material under thermal loading and rotational inertia with PDQ and FDQ methods and the effect of different mechanical boundary conditions, thermal field, angular velocity, and shell thickness on the stress distribution and displacement were investigated [13]. Arefi et al. presented the steady-state thermoelastic analysis for a (FG-CNTRC) cylindrical pressure vessel. They used the first-order shear deformation theory to drive and solve thermo-elastic static problems [14]. Gharooni and Ghannad analyzed hyperelastic cylindrical shells with variable thickness. The shell thickness and internal pressure were considered as arbitrary nonlinear profiles. To extract and solve the governing nonlinear equations, an effective combination of shear deformation theory and perturbation technique was used. They also investigated the effect of material properties, heterogeneity index, geometry, and pressure profiles on displacements and stresses [15]. Parhizkar and Ghannad presented the stable temperature and thermal strain distribution of the FGPM cylinder with the variable thickness using the first-order shear deformation theory [16]. Omidi et al. analyzed the deformation and transient thermal stress of a FGM rotating cylinder with a short length under thermal and mechanical loading, assuming the friction bed and the presence of external torque. They concluded that the radial displacement in the middle of a cylindrical shell is uniform, and its value decreases to zero with the increase of axial coordinates [17]. Benslimane et al. used Navier's second-order differential equation to calculate the mechanical displacements and stresses in a functionally graded materials thick-walled cylinder under pressure and heat flux. They investigated the effect of the thermal field, non-homogeneity parameter, and pressure on the thermoelasticity response of the cylinder [18]. Najibi et al. have presented a transient thermoelastic analysis for an axially symmetric FGM cylinder with finite length, considering the variations in material properties in the radial direction using power-law volume fraction and simple rule of mixture scheme. The mathematical solution method used was the higher-order graded finite element method [19]. Eliasi et al. presented the thermoelastic analysis of FGM conical shell under thermal shock. They derived the equations governing the shell based on shear deformation theory and solved the equations using the finite element method [20]. Using elasticity equations, Salehi and Ahmadi obtained the transient axisymmetric response of an FGM cylinder under thermal and mechanical loading. They also used the meshless local Petrov-Galerkin formulation for discretizing the equations and employed the Crank-Nicolson and Newmark methods for time integration [21]. Tokovyy studied the elastic and thermoelastic response of multi-layer heterogeneous hollow cylinders with characteristics of each layer with arbitrary distribution profiles in radial coordinates, based on the representation of material profiles in the entire set in the form of step-by-step variable functions with the concept of direct integration method towards the compatibility equation in terms of strain is checked [22]. Avey et al. presented the thermoelastic stability of carbon nanotube (CNT) patterned composite conical shells in the framework of shear deformation theory (SDT). The modified Dunnell-type shell theory is used to derive the basic equations for CNT patterned truncated conical shells. The Galerkin method is applied to the basic equations to find the critical temperature and critical axial load expressions for CNT patterned composite conical shells in the SDT framework. [23].

Ramezani et al. have presented a semi-analytical thermoelastic solution for a thick-walled cylinder with variable thickness under constant pressure using shear deformation theory and the disk-form multi-layer method [24]. Ghadimi and Ghannad analyzed the elasto-plastic stress of thick cylindrical shells under internal pressure using first-order and higher-order shear deformation theories, assuming the material to be elastic-perfectly plastic. They used the von Mises yield criterion and the radial return method to calculate plastic stress components. Their results showed that higher-order shear deformation theory provides more accurate stress predictions compared to first-order shear deformation theory [25]. Sofiyev and Avey modeled and solved the stability problem of laminated cylindrical shells formed from polymer-based nanocomposite layer. In that study, the stability behavior of laminated cylindrical shells consisting of carbon nanotube (CNT)–reinforced layers in thermal environment under the combined load is examined through extended shear deformation theory for the first time. Nanocomposite layers are modeled as homogeneous orthotropic and FG material [26].

The research conducted generally investigates the thermal behavior in the direction of the shell's thickness, while the direction of heat diffusion is in the cylindrical shell's radial and longitudinal directions. Also, the research on specific situations requires more analysis to generalize to general conditions. Taking into account bi-directional temperature field and the effect of shear stresses, the main objective of this study is to present an analytical solution for the calculation of stresses and displacements of a thick-walled cylinder subjected to two dimensional themoelasticity loads with internal pressure under various boundary conditions.

The thick cylindrical shell is subjected to thermal and pressure loadings in this research. The direction of heat flux propagation is considered along the radial and longitudinal directions. The cylindrical shell has been considered in two cases: mechanically clamped and fixed temperature and mechanically clamped and thermally insulated. Then, the governing equations were derived using the first-order shear deformation theory (FSDT) to determine the displacement field and first-order temperature theory (FTT) to determine the temperature field. The extracted equations have been analyzed using the perturbation technique (MAM).

2. Formulation and fundamental relations

In the shear deformation theory, the displacement of each point of the shell is not described by the displacement of the middle surface. Still, it is expressed by the sum of the middle surface's displacement and that point's displacement relative to the middle surface. In this theory, the displacement field of the crust around the middle layer is expressed using Taylor expansion with functions with variable coefficients. In general, the distance of each point from the shell to the axis of symmetry (r) is equal to the distance of the middle surface from the axis of symmetry (R) plus the distance of that point from the middle surface (z), in this case:

$$\mathrm{r} = \mathrm{R} + \mathrm{z}, \quad \left|\frac{\mathrm{z}}{\mathrm{R}}\right| < 1 \tag{1}$$

This will change the coordinate and differential component from r to z, and the displacement field of each shell point will be in the form of equation (2).

$$\begin{aligned} \mathrm{U_z} &= \mathrm{U_z}(\mathrm{z},\theta,\mathrm{x}) \\ \mathrm{U_\theta} &= \mathrm{U_\theta}(\mathrm{z},\theta,\mathrm{x}) \\ \mathrm{U_x} &= \mathrm{U_x}(\mathrm{z},\theta,\mathrm{x}) \end{aligned} \tag{2}$$

In equation (2) U_x, U_θ, U_z, the displacement field components are axial, circumferential, and radial, respectively. By rewriting the Taylor expansion, the components of the displacement field around the middle layer of the shell are obtained in the form of equation (3).

$$\begin{aligned} U_z &= U_z^0(x,\theta) + zU_z^1(x,\theta) + \cdots \\ U_\theta &= U_\theta^0(x,\theta) + zU_\theta^1(x,\theta) + \cdots \\ U_x &= U_x^0(x,\theta) + zU_x^1(x,\theta) + \cdots \end{aligned} \tag{3}$$

According to the above equations, the displacement is written as a polynomial in terms of z. Considering $z = 0$, it indicates the displacement of the shell's middle surface. If only the first term is considered, the analysis with a zero-order approximation of thick-walled shells is similar to the bending theory (first-order theory of thin shells). Suppose two terms of this expansion are considered. In that case, the analysis with the one-order approximation of thick-walled shells becomes similar to Flügge's theory (second-order theory of thin shells).

The first-order approximation theory is also known as Mirsky-Herman's first-order shear deformation theory. It is a generalization of Timoshenko's theory in beams and Mindlin's theory in plates.

In the first-order shear deformation theory (FSDT), the transverse shear strain distribution is constant in thickness, which leads to constant shear stress. The upper and lower surfaces of the shell do not tolerate shear, so the result is only a first approximation. The actual shear stress distribution varies through the thickness and has zero value along the top and bottom surfaces. For this reason, it is necessary to include a transverse shear correction factor in the equations.

The thick-walled axisymmetric cylindrical shell with inner radius r_i and outer radius r_o, length L, and thickness h is shown in Fig. 1; This shell is under heat flux H and pressure P loading on the inner surface.

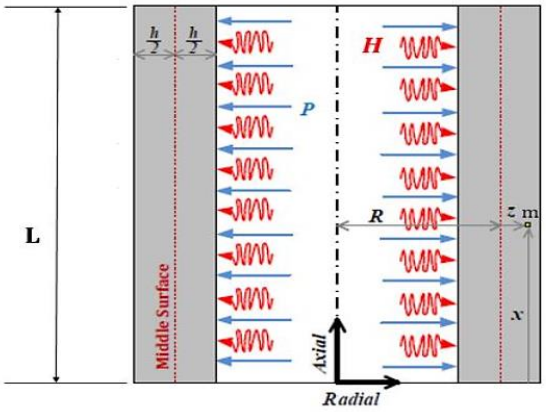


Fig. 1. Transverse section of the cylindrical shell under thermal and pressure

According to Fig. 1, the distance of the desired point (m) from the cylinder symmetry axis (r) is equal to the sum of the radius of the middle layer (R) and the distance of that point from the middle layer (z) as $r = R + z$. x is the distance of the arbitrary point m from the axis perpendicular to the symmetry axis of the cylinder. The parameters z and x must be within the ranges $-h/2 \le z \le h/2$ and $0 \le x \le L$, where h is the thickness of the cylinder.

The displacement field (U_z,U_x) governing the cylindrical shell and the variations of the temperature field ($\Theta = \Delta T = T - T^*$) compared to the ambient temperature are caused by thermal loading using the FSDT in the form of equation (4). T^* is reference temperature ($25^\circ C$). Given the geometric and material properties and loading conditions, the cylindrical shell is axially symmetric. As a result, variations in the circumferential $\left(\frac{\partial}{\partial\theta} = 0\right)$ direction are neglected. Therefore, the functions depend only on the radius (r) and axis (x) of the shell [27].

$$\begin{aligned} U_x(x,z) &= U_x^0(x) + zU_x^1(x) \\ U_\theta(x,z) &= 0 \\ U_z(x,z) &= U_z^0(x) + zU_z^1(x) \\ \Theta(x,z) &= \Theta^0(x) + z\Theta^1(x) \end{aligned} \tag{4}$$

In equation (4), the components $U_x^0(x)$ and $U_z^0(x)$ are the displacement components, and $\Theta^0(x)$ is the temperature parameter change on the middle surface. The functions $U_x^1(x)$, $U_z^1(x)$, and $\Theta^1(x)$ are used to determine displacement and temperature.

Strains can be represented as functions of displacement using equations (5) [3].

$$\begin{aligned}\varepsilon_x &= \frac{\partial U_x}{\partial x} = \frac{dU_x^0(x)}{dx} + z\frac{dU_x^1(x)}{x}\\ \varepsilon_\theta &= \frac{U_z}{r} = \frac{U_z^0(x) + zU_z^1(x)}{R+z}\\ \varepsilon_z &= \frac{\partial U_z}{\partial z} = U_z^1(x)\\ \gamma_{xz} &= \frac{\partial U_x}{\partial z} + \frac{\partial U_z}{\partial x} = U_x^1(x) + \frac{dU_z^0(x)}{dx} + z\frac{dU_z^1(x)}{dx}\end{aligned} \tag{5}$$

Thermal strains are expressed by the equations shown in (6).

$$\begin{aligned}e_x &= -\frac{\partial \Theta}{\partial x} = \frac{d\Theta^0(x)}{dx} - z\frac{d\Theta^1(x)}{dx}\\ e_z &= -\frac{\partial \Theta}{\partial z} = \Theta^1(x)\end{aligned} \tag{6}$$

Then, the stresses and heat flux are based on constitutive equations in the form of equations (7).

$$\begin{Bmatrix}\sigma_x\\ \sigma_\theta\\ \sigma_z\end{Bmatrix} = \frac{E}{(1-2\nu)(1+\nu)}\begin{bmatrix}1-\nu & \nu & \nu\\ \nu & 1-\nu & \nu\\ \nu & \nu & 1-\nu\end{bmatrix}\begin{Bmatrix}\varepsilon_x\\ \varepsilon_\theta\\ \varepsilon_z\end{Bmatrix} - \frac{E\alpha}{(1-2\nu)}\Theta\begin{Bmatrix}1\\1\\1\end{Bmatrix}$$
$$\tau_{xz} = \frac{E}{2(1+\nu)}\gamma_{xz} \tag{7-1}$$

$$\begin{bmatrix}h_x\\ h_z\end{bmatrix} = \begin{bmatrix}k & 0\\ 0 & k\end{bmatrix}\begin{bmatrix}e_x\\ e_z\end{bmatrix} \tag{7-2}$$

Young's modulus, Poisson's ratio, and thermal expansion coefficient are *E,* υ,α, respectively, and k is the thermal conductivity transfer coefficient. The effective stress resulting from the obtained stresses based on the von Mises yielding criteria is:

$$\sigma_{eff} = \frac{1}{\sqrt{2}}[(\sigma_x-\sigma_\theta)^2 + (\sigma_\theta-\sigma_z)^2 + (\sigma_z-\sigma_x)^2 + 6\tau_{xz}^2]^{0.5} \tag{8}$$

Then, the mechanical stress results (Equations (9) to (11)) and the thermal stress results (Equations (12) and (13)) are used to derive the governing equations.

$$\begin{Bmatrix}N_x^m\\ N_\theta^m\\ N_z^m\end{Bmatrix} = \int_{-\frac{h}{2}}^{\frac{h}{2}}\begin{Bmatrix}\sigma_x\left(1+\frac{z}{R}\right)\\ \sigma_\theta\\ \sigma_z\left(1+\frac{z}{R}\right)\end{Bmatrix}dz \tag{9}$$

$$\begin{Bmatrix}M_\theta^m\\ M_x^m\end{Bmatrix} = \int_{-\frac{h}{2}}^{\frac{h}{2}}\begin{Bmatrix}\sigma_\theta\\ \sigma_x\left(1+\frac{z}{R}\right)\end{Bmatrix}z\,dz \tag{10}$$

$$\begin{Bmatrix}Q_x^m\\ M_{xz}^m\end{Bmatrix} = \int_{-\frac{h}{2}}^{\frac{h}{2}}\begin{Bmatrix}h_z\\ h_x\end{Bmatrix}\left(1+\frac{z}{R}\right)dz \tag{11}$$

$$M_x^t = \int_{-\frac{h}{2}}^{\frac{h}{2}} h_x\left(1+\frac{z}{R}\right)z\,dz \tag{12}$$

$$\begin{Bmatrix} N_x^t \\ N_z^t \end{Bmatrix} = \int_{-\frac{h}{2}}^{\frac{h}{2}} \begin{Bmatrix} h_x \\ h_z \end{Bmatrix} \left(1 + \frac{z}{R}\right) dz \tag{13}$$

First, the virtual work principle is used to derive the system's governing equations. For this purpose, the strain energy density of the system (14) is calculated [28].

$$\begin{aligned} U &= \int_0^L \int_0^{2\pi} \int_{r_i}^{r_o} U^* \, dV \\ dV &= r dr d\theta dx = (R+z) dz d\theta dx \qquad 0 \le \theta \le 2\pi; \;\; 0 \le x \le L \\ U^* &= \frac{1}{2}\sigma_{ij}\varepsilon_{ij} = \frac{1}{2}(\sigma_x\varepsilon_x + \sigma_\theta\varepsilon_\theta + \sigma_z\varepsilon_z + \tau_{xz}\gamma_{xz} - h_x e_x - h_z e_z) \\ \frac{\delta U}{2\pi} &= \int_0^L R \int_{-h/2}^{h/2} (\sigma_x\delta\varepsilon_x + \sigma_\theta\delta\varepsilon_\theta + \sigma_z\delta\varepsilon_z + \tau_{xz}\delta\gamma_{xz} - h_z\delta e_z - h_x\delta e_x)\left(1 \right. \\ &\qquad \left. + \frac{z}{R}\right) dz \, dx \end{aligned} \tag{14}$$

Then, by substituting the stress results into equations (9) to (13), the strain energy of the system is obtained as follows:

$$\begin{aligned} \frac{\delta U}{2\pi} = \int_0^L R \Bigg[& N_x^m \frac{d(\delta U_x^0)}{dx} + M_x^m \frac{d(\delta U_x^1)}{dx} + \frac{1}{R(x)} N_\theta^m (\delta U_z^0) + \frac{1}{R(x)} M_\theta^m (\delta U_z^1) \\ & + N_z^m (\delta U_z^1) + Q_x^m (\delta U_x^1) + Q_x^m \frac{d(\delta U_z^0)}{dx} + M_{xz}^m \frac{d(\delta U_z^1)}{dx} + N_x^t \frac{d(\delta\Theta^0)}{dx} \\ & + M_x^t \frac{d(\delta\Theta^1)}{dx} + N_z^t (\delta\Theta^1) \Bigg] dx \end{aligned} \tag{15}$$

In the continuation of the work of external forces, the internal pressure (P) and internal heat flux (H) effective on the inner and outer surfaces of the cylindrical shell are obtained as in equation (16) [29].

$$\begin{aligned} W &= \int_0^L \int_0^{2\pi} (P U_z - H\Theta|) \, dS \;, \; \mathrm{dS} = r_i d\theta dx = \left(R - \frac{h}{2}\right) d\theta dx \\ \frac{\delta W}{2\pi} &= \int_0^L \left(\left[P(\delta U_z^0 + z\delta U_z^1) - H_i(\delta\Theta^0 + z\delta\Theta^1)|_{r_i} \right] \left(R - \frac{h}{2}\right) \right) dx \end{aligned} \tag{16}$$

Using the principle of virtual work and equalizing the work changes of external forces and kinetic energy changes, the governing differential equations of the system are obtained according to equations ((17) and (18)).

$$\frac{\delta U}{2\pi} = \frac{\delta W}{2\pi} \tag{17}$$

$$\begin{aligned} & N_x^m = k_4 \\ & -R\frac{dM_x^m}{dx} + RQ_x^m = 0 \\ & -R\frac{dQ_x^m}{dx} + N_\theta^m = P\left(R - \frac{h}{2}\right) \\ & -R\frac{dM_{xz}^m}{dx} + M_\theta^m + R(x)N_z^m = -P\frac{h}{2}\left(R - \frac{h}{2}\right) \end{aligned} \tag{18-1}$$

$$N_x^t = f_1(x), f_1(x) = -\frac{1}{R}H_i\left(R-\frac{h}{2}\right)x + k_2$$
$$-R\frac{dM_x^t}{dx} + R(x)N_z^t = f_2, f_2 = H_i\left(R-\frac{h}{2}\right) \quad (18\text{-}2)$$

The boundary conditions of the problem are also obtained by setting the remaining sentences to zero in the form of equation (19):

$$[R(N_x^m\delta U_x^0 + M_x^m\delta U_x^1 + Q_x^m\delta U_z^0 + M_{xz}^m\delta U_z^1 + N_x^t\delta\Theta^0 + M_x^t\delta\Theta^1)]_{0,L} = 0 \quad (19)$$

The matrix of coefficients and the force vector of the governing equations $[A^*]_{6\times6}, [B^*]_{6\times6}, [C^*]_{6\times6}, \{F^*\}$ are as follows:

$$[A^*]=\begin{bmatrix} 0 & 0 & 0 & 0 & B_{15} & 0 \\ 0 & A_{22} & 0 & 0 & 0 & 0 \\ 0 & 0 & A_{33} & A_{34} & C_{35} & 0 \\ 0 & 0 & A_{43} & A_{44} & C_{45} & 0 \\ 0 & 0 & 0 & 0 & 0 & 0 \\ 0 & 0 & 0 & 0 & 0 & A_{66} \end{bmatrix} \quad (20)$$

$$[B^*]=\begin{bmatrix} 0 & A_{12} & 0 & 0 & 0 & 0 \\ A_{21} & 0 & B_{23} & B_{24} & 0 & B_{26} \\ 0 & B_{32} & 0 & 0 & 0 & 0 \\ 0 & B_{42} & 0 & 0 & 0 & 0 \\ 0 & 0 & 0 & 0 & 0 & A_{56} \\ 0 & 0 & 0 & 0 & A_{65} & 0 \end{bmatrix} \quad (21)$$

$$[C^*]=\begin{bmatrix} A_{11} & 0 & B_{13} & B_{14} & 0 & 16 \\ 0 & C_{22} & 0 & 0 & B_{25} & 0 \\ B_{31} & 0 & C_{33} & C_{34} & 0 & 0 \\ B_{41} & 0 & C_{43} & C_{44} & 0 & C_{36} \\ 0 & 0 & 0 & 0 & A_{55} & 0 \\ 0 & 0 & 0 & 0 & 0 & C_{66} \end{bmatrix} \quad (22)$$

$$\{F^*\} = \begin{Bmatrix} \frac{k_4}{h^2} \\ 0 \\ \frac{P}{\lambda E}\left(R-\frac{h}{2}\right) \\ \frac{Ph}{2\lambda E}\left(R-\frac{h}{2}\right) \\ f_1 \\ f_2 \end{Bmatrix} \quad (23)$$

The resulting equations are a system of heterogeneous linear equations with constant coefficients, and the perturbation technique has been used to solve them.

$$[A^*]\frac{d^2}{dx^2}\{y\} + [B^*]\frac{d}{dx}\{y\} + [C^*]\{y\} = \{F^*\}$$
$$\{y\} = \{U_x^0 \quad U_x^1 \quad U_z^0 \quad U_z^1 \quad \Theta^0 \quad \Theta^1\}^T \quad (24)$$

To solve the governing equations with the help of the perturbation technique, the extracted equations must first be converted into dimensionless; the dimensionless parameters are defined as follows should be written instead of (25).

$$\epsilon = \frac{h_0}{L}, h^* = \frac{h}{h_0}, R^* = \frac{R}{h_0}, x^* = \frac{x}{L}, K^* = \frac{K}{K_m}, \Theta^{0^*} = \Theta^0\alpha_m, \Theta^{1^*} = \Theta^1\alpha_m h_0,$$
$$F^{1^*} = F^1\frac{\alpha_m}{K_m}, F^{2^*} = F^2\frac{\alpha_m}{h_0K_m}, U_x^{0^*} = \frac{U_x^0}{L}, U_z^{0^*} = \frac{U_z^0}{L} \quad (25)$$

The coefficients α_m and K_m are the coefficient of thermal expansion and thermal conductivity of the inner layer of the cylindrical shell, respectively, and ϵ is a small parameter by substituting the dimensionless parameters in the extracted equations, the dimensionless equations governing the cylindrical shell are obtained, which are as follows:

$$\epsilon\left[R^*h^*(1-\upsilon)\frac{dU_x^{0^*}}{dx^*}+(1-\upsilon)\frac{h^{*3}}{12}\frac{d^2U_x^{1^*}}{dx^{*2}}\right]+\upsilon h^*U_z^{0^*}+\upsilon R^*h^*U_z^{1^*}-R^*h^*(1+\upsilon)\Theta^{0^*} -\frac{h^{*3}}{12}(1+\upsilon)\Theta^{1^*}=k_1^* \tag{26}$$

$$\epsilon^2\left[-(1-\upsilon)\frac{h^{*3}}{12}\frac{d^2U_x^{0^*}}{dx^{*2}}+(1-\upsilon)\frac{R^*h^{*3}}{12}\frac{d^2U_x^{1^*}}{dx^{*2}}\right] +\epsilon\left[\mu R^*h^*\frac{dU_z^{0^*}}{dx^*}+(\mu-2\upsilon)\frac{h^{*3}}{12}\frac{dU_z^{1^*}}{dx^*}+(1+\upsilon)\frac{h^{*3}}{12}\frac{d\Theta^{0^*}}{dx^*}\right. \left.+(1+\upsilon)\frac{R^*h^{*3}}{12}\frac{d\Theta^{1^*}}{dx^*}\right]+\mu R^*h^*U_x^{1^*}=0 \tag{27}$$

$$\epsilon^2\left[-\mu R^*h^*\frac{d^2U_z^{0^*}}{dx^{*2}}+\frac{\mu h^{*3}}{12}\frac{d^2U_z^{1^*}}{dx^{*2}}\right]+\epsilon\left[\upsilon h^*\frac{dU_x^{0^*}}{dx^*}-\mu R^*h^*\frac{dU_z^{1^*}}{dx^*}\right]+\beta(1-\upsilon)U_z^0 +[(1-\upsilon)\beta R^*-h^*]U_z^1-h^*(1+\upsilon)\Theta^{0^*}=\frac{P}{\lambda E}\left(R^*-\frac{h^*}{2}\right) \tag{28}$$

$$\epsilon^2\left[-\frac{\mu h^{*3}}{12}\frac{d^2U_z^{0^*}}{dx^{*2}}-\frac{\mu R^*h^{*3}}{12}\frac{d^2U_z^{1^*}}{dx^{*2}}\right]+\epsilon\left[\upsilon R^*h^*\frac{dU_x^{0^*}}{dx^*}-(\mu-2\nu)\frac{h^{*3}}{12}\frac{dU_x^{1^*}}{dx^*}\right] +\beta(1-\upsilon)R^{*^2}U_z^{1^*}-[(1-\upsilon)\beta R^*-h^*]U_z^0-R^*h^*(1+\upsilon)\Theta^{0^*} -\frac{h^{*3}}{6}(1+\upsilon)\Theta^{1^*}=\frac{Ph^*}{2\lambda E}\left(R^*-\frac{h^*}{2}\right) \tag{29}$$

$$\epsilon\left[-K^*h^*\frac{d\Theta^{0^*}}{dx^*}-\frac{K^*h^{*3}}{12R^*}\frac{d\Theta^{1^*}}{dx^*}\right]=f_1^* \tag{30}$$

$$\epsilon^2\left[\frac{K^*h^{*3}}{12}\frac{d^2\Theta^{0^*}}{dx^{*2}}+\frac{K^*R^*h^{*3}}{12}\frac{d^2\Theta^{1^*}}{dx^{*2}}\right]-K^*R^*h^*\Theta^{1^*}=f_2^* \tag{31}$$

By assuming $V=\frac{dU_x^0}{dx}\rightarrow V=\epsilon\frac{dU_x^{0^*}}{dx^*}\rightarrow U_x^{0^*}=\frac{1}{\epsilon}\int Vdx^*+k_5$ and $\epsilon\frac{d\Theta^{0^*}}{dx^*}=\xi^*\rightarrow\Theta^{0^*}=\frac{1}{\epsilon}\int\xi^*dx^*+k_3$, the dimensionless equations (30) and (31) become equations (32) and (33):

$$-K^*h^*\xi^*+\epsilon\frac{K^*h^{*3}}{12R^*}\frac{d\Theta^{1^*}}{dx^*}=f_1^* \tag{32}$$

$$\epsilon^2\frac{K^*R^*h^{*3}}{12}\frac{d^2\Theta^{1^*}}{dx^{*2}}+\epsilon\frac{K^*h^{*3}}{12}\frac{d\xi^*}{dx^*}-K^*R^*h^*\Theta^{1^*}=f_2^* \tag{33}$$

The set of dimensionless equations is obtained as follows (34).

$$y=\left\{V\quad U_x^1\quad U_z^{0^*}\quad U_z^1\quad \xi^*\quad \Theta^{1^*}\right\}^T \qquad \epsilon^2[A_1^*]\frac{d^2}{dx^2}\{y^*\}+\epsilon[B_1^*]\frac{d}{dx}\{y^*\}+[C_1^*]\{y^*\}=\{F_1^*\} \tag{34}$$

In the dimensionless equations governing the system, the order of the two-degree equations is reduced by setting the perturbation parameter equal to zero. According to the MAM as a perturbation technique, they become algebraic equations, which shows that the problem contains two boundary layers at the two ends of the cylindrical shell. The equations' solutions include an outer solution in the areas far from the borders, and the other solution is around the borders (cylindrical shell edges).

$$\{y^*\} = \{y^*_{out}\} + \{y^*_{in}\} - \{U_{over}\}$$
$$\{y^*_{in}\} = \{y^*_{in(0)}\} + \{y^*_{in(L)}\} \quad (35)$$
$$\{U_{over}\} = \{U_0\} + \{U_L\}$$

3. Solution

In order to solve the equations governing the thick-walled cylindrical shell, with the help of the matched asymptotic expansion method of perturbation theory, the equations are converted into a group of equations with constant coefficients. The equations' external solutions, which are far from the shell's boundaries and middle, are extracted. In the next part, the solution in The boundaries includes the solution on the left boundary $(x = 0)$ and the solution on the right boundary $(x = L)$. Finally, the general solution of the problem, which includes the external solution and the solution at the boundaries and the overlapping areas of the external solution and the solution at the boundaries, is presented.

3.1. Outer solution

The outer solution is considered a uniform series of perturbation terms (ϵ). By substituting equation (36) into the general equation (34) and separating the coefficients of approximation of zero and approximation of an external solution of the equation is extracted.

$$y^*_{out} = \sum_{n=0}^{\infty} \epsilon^n y_n(x^*) = y_0 + \epsilon y_1 + \cdots \quad (36)$$

$$y^*_{out}(x^*) = y_0(x^*) + \epsilon y_1(x^*)$$
$$\begin{cases} y_0 = \left\{ {U_z^{0^*}}_0(x^*) \quad U^1_{z_0} \quad V_0(x^*) \quad U^1_{x_0} \quad \xi^*_0(x^*) \quad \Theta^{1^*}_0(x^*) \right\}^T \\ y_1 = \left\{ {U_z^{0^*}}_1(x^*) \quad U^1_{z_1} \quad V_1(x^*) \quad U^1_{x_1} \quad \xi^*_1(x^*) \quad \Theta^{1^*}_1(x^*) \right\}^T \end{cases} \quad (37)$$

By solving the equations (37) and (38), the solution set $\{y_0\}$ and $\{y_1\}$ were obtained for the external solution and away from the border areas.

$$o(\epsilon^0): [C^*_1]\{y_0\} = \{f^*\}$$
$$\begin{cases} \upsilon h^* {U_z^{0^*}}_0 + R^* \upsilon h^* U^1_{z_0} + R^* h^* (1-\upsilon) V_0 - \dfrac{h^{*3}}{12}(1+\upsilon)\Theta^{1^*}_0 - k_4 = 0 \\ \mu R^* h^* {U_z^{0^*}}_1 + \dfrac{h^{*3}}{12}(1+\upsilon)\xi^*_0 = 0 \\ \beta(1-\upsilon){U_z^{0^*}}_0 + (h^* - (1-\upsilon)R^*\beta)U^1_{z_0} + \upsilon h^* V_0 - \dfrac{P\left(R^* - \frac{h^*}{2}\right)}{\lambda E} = 0 \\ (h^* - (1-\upsilon)R^*\beta){U_z^{0^*}}_0 + (1-\upsilon)R^{*2}\beta U^1_{z_0} + \upsilon R^* h^* V_0 - \dfrac{h^{*3}}{6}(1+\upsilon)\Theta^{1^*}_0(x^*) + \dfrac{P\left(R^* - \frac{h^*}{2}\right)}{\lambda E} = 0 \\ -K_s h^* \xi^*_0 - f^*_1 = 0 \\ -K_s R^* h^* \Theta^{1^*}_0 - f^*_2 = 0 \end{cases} \quad (38)$$

$$o(\epsilon^1): [C^*_1]\{y_1\} + [B^*_1]\left\{\frac{dy_0}{dx^*}\right\} = \{0\} \quad (39)$$

$$\begin{cases} \upsilon h^* U_z^{0^*}{}_1 + R^* \upsilon h^* U_{z\,1}^1 + R^* h^* (1-\upsilon) V_1 - \dfrac{h^{*3}}{12}(1+\upsilon)\Theta_1^{1^*} + \dfrac{h^{*3}}{12}(1-\upsilon)\left(\dfrac{dU_{x\,1}^1}{dx}\right) = 0 \\ \mu R^* h^* U_z^{0^*}{}_1 + \dfrac{h^{*3}}{12}(1+\upsilon)\xi_1^* + \mu R^* h^* \left(\dfrac{dU_z^{0^*}{}_1}{dx}\right) + \dfrac{h^{*3}}{12}(1+\upsilon)\left(\dfrac{dU_{z\,1}^1}{dx}\right) - \dfrac{h^{*3}}{12}(1-\upsilon)\left(\dfrac{dV_1}{dx}\right) + \dfrac{R^* h^{*3}}{12}(1+\upsilon)\left(\dfrac{d\Theta_1^{1^*}}{dx}\right) = 0 \\ \beta(1-\upsilon)U_z^{0^*}{}_0 + (h^* - (1-\upsilon)R^*\beta)U_z^{0^*}{}_1 + \upsilon h^* V_0 - \dfrac{P\left(R^* - \dfrac{h^*}{2}\right)}{\lambda E} = 0 \\ -\dfrac{h^{*3}}{6}(1+\upsilon)\Theta_1^{1^*} - (\mu - 2\upsilon)\dfrac{h^{*3}}{12}\left(\dfrac{dU_{x\,1}^1}{dx}\right) = 0 \\ -K_s h^* \xi_1^* - \dfrac{K_s h^{*3}}{12R^*}\left(\dfrac{d\Theta_1^{1^*}}{dx}\right) = 0 \\ -K_s R^* h^* \Theta_1^{1^*} + \dfrac{K_s h^{*3}}{12R^*}\left(\dfrac{d\xi_1^*}{dx}\right) = 0 \end{cases}$$

3.2. Inner solution at the lower boundary ($x^* = 0$):

Based on the matched asymptotic expansion perturbation technique, we need two solutions consisting of the solution in the regions far from the boundaries and the other solution at the first and last boundaries of the cylindrical shell, which was extracted in the previous part of the solution in the region far from the boundaries and in this part, The solution at the lower boundary of the cylindrical shell is discussed. The fast parameter is used to solve at the boundaries, and using this parameter at the lower boundary, we have $\eta = \dfrac{x^*}{\epsilon}$ and Taylor expansion for loadings and displacement coefficients, and a temperature at the boundary $x^* = 0$:

$$\begin{cases} A_i^*(x^*) = A_0^* + \epsilon\eta dA_0 + \cdots;\ A_0^* = A_i^*(0), dA_0 = \left.\dfrac{dA_i^*}{dx^*}\right|_{x^*=0} \\ F^*(x^*) = F_0^* + \epsilon\eta dF_0 + \cdots;\ F_0^* = F^*(0), dF_0 = \left.\dfrac{dF^*}{dx^*}\right|_{x^*=0} \end{cases} \tag{40}$$

These are obtained by substituting the Taylor expansion in the governing equations of the problem and separating the coefficients of order zero and order of one parameter epsilon of the governing equations at the boundary $x^* = 0$.

$$y_{in(0)}^* = Y_{0i} + \epsilon Y_{1i}$$

$$Y_{0i} = \begin{Bmatrix} U_{0\,0i}^z(\eta) \\ U_{1\,0i}^z(\eta) \\ V_{0i}(\eta) \\ U_{1\,0i}^x(\eta) \\ \zeta_{0i}(\eta) \\ \Theta_{0i}^1(\eta) \end{Bmatrix}; Y_{1i} = \begin{Bmatrix} U_{0\,1i}^z(\eta) \\ U_{1\,1i}^z(\eta) \\ V_{1i}(\eta) \\ U_{1\,1i}^x(\eta) \\ \zeta_{1i}(\eta) \\ \Theta_{1i}^1(\eta) \end{Bmatrix} \tag{41}$$

$$O(\epsilon^0) \longrightarrow L(V_0, \eta|0) = \{F_{0i}^*(0)\}$$

$$L(*, \eta|0) = [D_2^*(0)]\frac{d^2\{*\}}{d\eta^2} + [D_1^*(0)]\frac{d\{*\}}{d\eta} + [D_0^*(0)]\{*\}$$

$$[D_2^*(0)] = \begin{bmatrix} 0 & 0 & 0 & 0 & D_{2i_{15}} & 0 \\ 0 & 0 & 0 & D_{2i_{24}} & 0 & 0 \\ D_{2i_{31}} & D_{2i_{32}} & 0 & 0 & D_{2i_{35}} & 0 \\ D_{2i_{41}} & D_{2i_{42}} & 0 & 0 & D_{2i_{45}} & 0 \\ 0 & 0 & 0 & 0 & 0 & 0 \\ 0 & 0 & 0 & 0 & 0 & D_{2i_{66}} \end{bmatrix}; [D_1^*(0)] = \begin{bmatrix} 0 & 0 & 0 & D_{1i_{14}} & 0 & 0 \\ D_{1i_{21}} & D_{1i_{22}} & D_{1i_{23}} & 0 & 0 & D_{1i_{26}} \\ 0 & 0 & 0 & D_{1i_{34}} & 0 & 0 \\ 0 & 0 & 0 & D_{1i_{44}} & 0 & 0 \\ 0 & 0 & 0 & 0 & 0 & D_{1i_{56}} \\ 0 & 0 & 0 & 0 & D_{1i_{65}} & 0 \end{bmatrix} \tag{42}$$

$$[D_0^*(0)] = \begin{bmatrix} D_{0i_{11}} & D_{0i_{12}} & D_{0i_{13}} & 0 & 0 & D_{0i_{16}} \\ 0 & 0 & 0 & D_{0i_{24}} & D_{0i_{25}} & 0 \\ D_{0i_{31}} & D_{0i_{32}} & D_{0i_{33}} & 0 & 0 & 0 \\ D_{0i_{41}} & D_{0i_{42}} & D_{0i_{43}} & 0 & 0 & D_{0i_{46}} \\ 0 & 0 & 0 & 0 & D_{0i_{55}} & 0 \\ 0 & 0 & 0 & 0 & 0 & D_{0i_{66}} \end{bmatrix}; \{F_{0i}^*(0)\} = \begin{Bmatrix} F_{0i_0}^* \\ F_{0i_1}^* \\ F_{0i_2}^* \\ F_{0i_3}^* \\ F_{0i_4}^* \\ F_{0i_5}^* \end{Bmatrix}$$

The matrixes $[D_i^*(0)]$ are the coefficients matrix of the displacement and temperature parameters at the bottom boundary of the cylindrical shell, and $\{F_{oi}^*(0)\}$ the vector of forces and inhomogeneity of the equations governing the system at the bottom boundary of the cylindrical shell. To solve the set of inhomogeneous equations governing the system, first, the general governing solution is considered$\{Y\} = \{V_i\}e^{\lambda_i \eta}$, which is the form, λ_i eigenvalue, and $\{V_i\}$ eigenvector corresponding to the eigenvalue obtained for the homogeneous equations governing the system.

$$[C]_{6\times6}\{V_i\} = \{0\};\quad [C] = \lambda_i^2[D_{2i}] + \lambda_i[D_{1i}] + [D_{0i}] \tag{43}$$

To obtain the eigenvalues, by setting the determinant of the matrix of coefficients to zero $(det[C] = 0)$, the characteristic equations are obtained, and the resulting equation is an algebraic equation of the sixth order, which the eigenvalues are obtained by solving this equation of order six. The values with negative real part coefficients have been selected according to the equation's solution in the cylindrical shell's bottom boundary. Then, eigenvalues and eigenvectors were obtained. Then, the inhomogeneity part of the equations is solved according to the inhomogeneity part of the solution, which is extracted as an equation (44).

$$\begin{aligned} &\{Y_{0i}\}_g = \sum_{i=1}^{6} C_i\{V\}_i e^{\lambda_i \eta} \\ &\{Y_{0i}\}_p = \{K_0\} \longrightarrow [D_0^*(0)]\{K_0\} = \{F_{0i}^*(0)\} \longrightarrow \{K_0\} = [D_0^*(0)]^{-1}\{F_{0i}^*(0)\} \end{aligned} \tag{44}$$

The solution of the order of an epsilon parameter includes a general solution of the homogeneous equations, and the private solution of the equations contains the inhomogeneous part, which is this general solution similar to the general solution of the zero order of the eigenvalue problem. The private solution of the equation includes a power function of η, which is obtained by substituting the coefficients $\{K_0\}$ and $\{K_1\}$ in the set of heterogeneous equations.

$$\begin{aligned} &O(\epsilon^1) \longrightarrow L(V_1, \eta|0) = \eta\left\{\frac{dF_{0i}^*}{dx^*}\right\}\Big|_0 \\ &\{Y_{1i}\}_g = \sum_{i=1}^{6} C_i\{V\}_i e^{m_i \eta} \\ &\left.\begin{aligned} &\{Y_{1i}\}_p = \{K_0\} + \eta\{K_1\} \\ &\eta\left\{\frac{dF^*}{dx^*}\right\}\Big|_{x^*=0} = B_0 + B_1\eta \end{aligned}\right\} \\ &\qquad\longrightarrow \begin{cases} [D_0^*(0)]\{K_1\} = \{B_1\} \\ [D_0^*(0)]\{K_0\} + [D_1^*(0)]\{K_1\} = \{B_1\} \end{cases} \end{aligned} \tag{45}$$

3.3. Inner solution at the upper boundary ($x^* = 1$):

As stated in the previous section, the fast parameter is used to solve the upper boundary of the cylindrical shell, which is considered as the variable in the upper boundary $\zeta = \frac{x^*-1}{\varepsilon}$, and we have the Taylor expansion of the loadings and the matrix of coefficients in the boundary $x^* = 1$:

$$\begin{cases} A_i^*(x^*) = A_1^* + \epsilon\eta dA_1 + \cdots; A_1^* = A_i^*(1), dA_1 = \left.\dfrac{dA_i^*}{dx^*}\right|_{x^*=1} \\ F^*(x^*) = F_1^* + \epsilon\eta dF_1 + \cdots; F_1^* = F^*(1), dF_1 = \left.\dfrac{dF^*}{dx^*}\right|_{x^*=1} \end{cases} \tag{46}$$

These are obtained by substituting the Taylor expansion in the governing equations of the problem and separating the coefficients of order zero and order one epsilon parameter of the governing equations in the boundary $x^* = 1$.

$$y^*_{in(1)} = Y_{0I} + \epsilon Y_{1I}$$

$$Y_{0I} = \begin{Bmatrix} U^z_{0\,0I}(\eta) \\ U^z_{1\,0I}(\eta) \\ V_{0I}(\eta) \\ U^x_{1\,0I}(\eta) \\ \zeta_{0I}(\eta) \\ \Theta^1_{0I}(\eta) \end{Bmatrix}; Y_{1I} = \begin{Bmatrix} U^z_{0\,1I}(\eta) \\ U^z_{1\,1I}(\eta) \\ V_{1I}(\eta) \\ U^x_{1\,1I}(\eta) \\ \zeta_{1I}(\eta) \\ \Theta^1_{1I}(\eta) \end{Bmatrix} \quad (47)$$

$$O(\epsilon^0) \longrightarrow L(W_0, \xi|0) = \{F^*_{0I}(1)\}$$

$$L(*, \xi|0) = [D^*_2(1)]\frac{d^2\{*\}}{d\xi^2} + [D^*_1(1)]\frac{d\{*\}}{d\xi} + [D^*_0(1)]\{*\} \quad (48)$$

The solution at the upper boundary of the cylindrical shell includes the zero order and first-order of epsilon. The zero-order solution, similar to the solution in the lower bound, contains a general solution and another solution of the inhomogeneity part. The general solution of an eigenvalue problem is that the eigenvalues are obtained by setting the determinant of the matrix of coefficients equal to zero and solving the extracted characteristic equation, with the condition that the eigenvalues have negative coefficients of the real part and the private solution takes into account the inhomogeneity part. Similar to the extracted lower bound. Then, the solution of the order of one epsilon includes general and private solutions. The general solution is identical to the zero-order general solution, and the private solution consists of the power function considered for the private solution $\{V_1\}_p = \{K_0\} + \zeta\{K_1\}_p$. They are extracted by inserting the coefficients.

3.4. Composite solution

According to the perturbation theory, the set of solutions far from the border areas and the solution in the border areas can be obtained by obtaining the combined solution, which includes the sum of the external solution and the solutions of the border areas minus the overlapping parts. The composite solution is then extracted.

$$Y_{composite} = Y_{outer} + Y_{in(0)} + Y_{in(L)} - (Y_{outer})^{inner} - (Y_{outer})^{inner} \quad (49)$$

$(Y_{outer})^{inner}$ The standard part of internal and external solutions are in the boundary regions, obtained according to Van Dyck's matching principle (source 47). By integrating the third parameter of the composite solution, the function $U^{0^*}_{x\,0}(x^*)$($U^{0^*}_{x\,0}(x^*) = \frac{1}{\epsilon}\int V(x^*)dx^* + k_5$) and integrating the fifth parameter of the combined solution, the function $\Theta^{0^*}(x^*)(\Theta^{0^*}(x^*) = \frac{1}{\varepsilon}\int \zeta^* dx^* + k_3$) are obtained. Finally, by substituting the boundary conditions of the two ends of the cylindrical shell, the values k_1, k_2, k_3, k_4 have been obtained.

4. Results and discussion

For the numerical analysis of a thick-walled cylinder under pressure and thermal loading, the geometrical parameters are as follows: inner radius $r_i = 40\ mm$, outer radius $r_o = 60\ mm$, and cylinder length $L = 800\ mm$. Elastic Young's modulus, coefficient of thermal expansion, coefficient of thermal conductivity of cylindrical shell $E = 200\ GPa$, $\alpha = 12 * 10^{-6}\ 1/℃$ and $k = 45\ W/m℃$ and Poisson's ratio equal with 0.3. The inner surface of the cylindrical shell is under pressure loading $P = 80\ MPa$ and heat flux $H_i = 500\ W/m^2$. The reference temperature for both cases is $T^* = 25$ ℃. The dimensionless data of graphs are defined as follows:

$$\bar{x} = \left(\frac{x}{L}\right), \bar{r} = \left(\frac{r}{r_i}\right), \bar{U}_z = \left(\frac{U_z}{h}\right) * 10^4, \bar{U}_x = \left(\frac{U_x}{h}\right) * 10^4, \bar{T} = \left(\frac{T}{T^*}\right), \bar{\sigma}_\theta = \left(\frac{\sigma_\theta}{P}\right) \quad (50)$$

$$\tau_{zx} = \left(\frac{\tau_{zx}}{P}\right), \bar{\sigma}_{eff} = \left(\frac{\sigma_{eff}}{P}\right)$$

4.1. Clamped-clamped boundary condition

In the first case, the beginning and end of the cylindrical shell are fixed and under a temperature of T=25℃. Then, the mechanical and thermal behaviors of the cylindrical shell, along with its thickness and longitudinal direction, were analyzed.

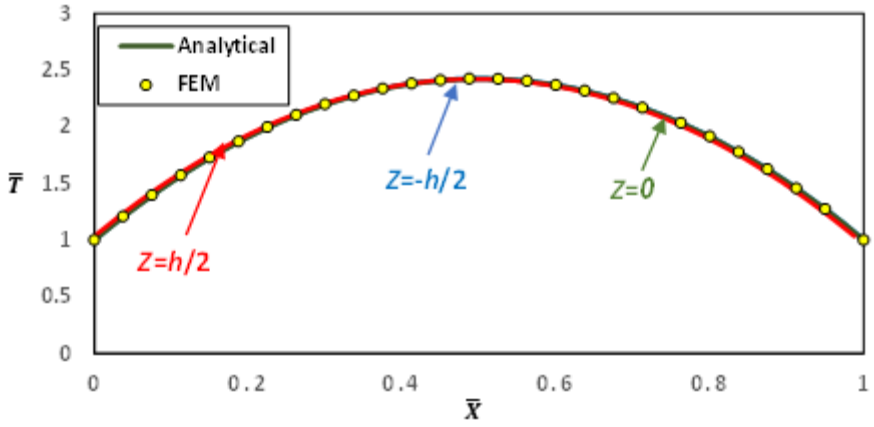


Fig. 2. Temperature distribution along the cylindrical shell

Figure 2 shows the temperature distribution in the axial direction of the shell for three layers. The maximum temperature value occurred in the middle axis of the cylindrical shell, and the change in the cylindrical shell layer does not affect the temperature field. Figs.3 and 4 show the distribution of axial and radial displacement in the cylindrical shell.

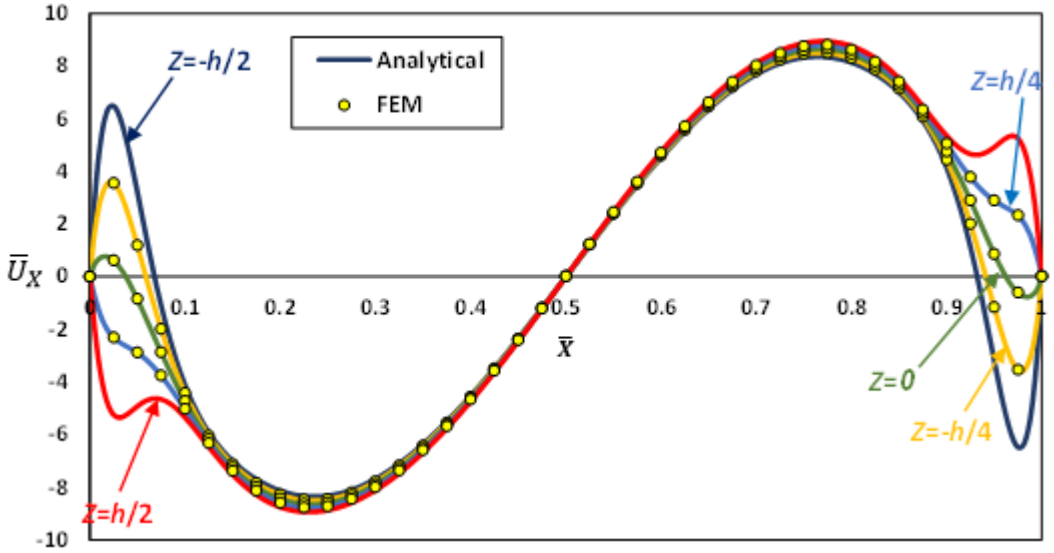


Fig. 3. Axial displacement distribution along the cylindrical shell

As seen in Fig. 3, the cylindrical shell's axial displacement values agree well with the finite element simulation. The maximum axial displacement occurred in the areas near the boundaries and became zero in the middle part of the shell. The axial displacement is somewhat independent of the radial direction and varies primarily along the axial direction.

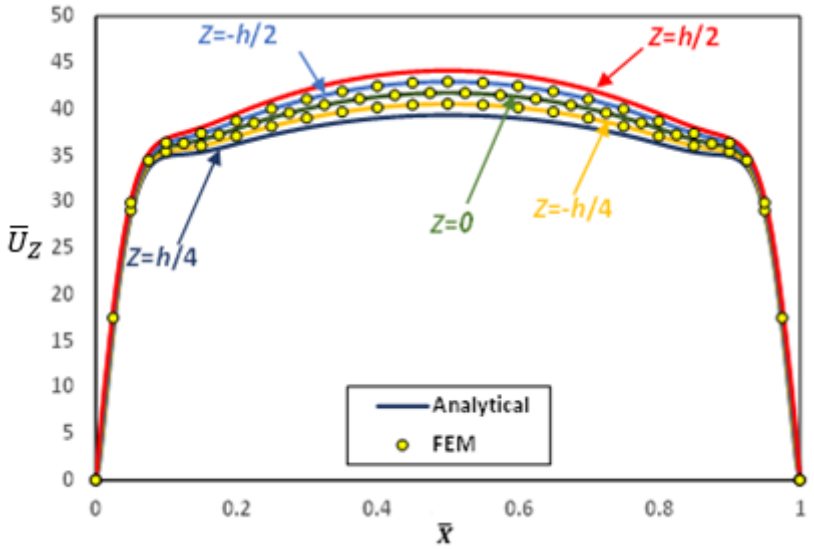


Fig. 4. Radial displacement distribution along the cylindrical shell

As shown, the most significant radial displacement occurred in the areas far from the borders and in the middle of the cylindrical shell, and these values changed with the change of the shell layers.

The following presents the distribution of circumferential and radial stress for different layers of the cylindrical shell along its length. The peak changes of these stresses occur at the boundaries of the shell and have constant values in the middle areas of the shell.

The investigation of circumferential, radial, shear, and effective stresses in different layers of the cylinder is done in Figs. 5-8. The Distribution of axial and radial displacements, and temperature in different layers of the thickness and length of the cylinder is done in Fig. 9.

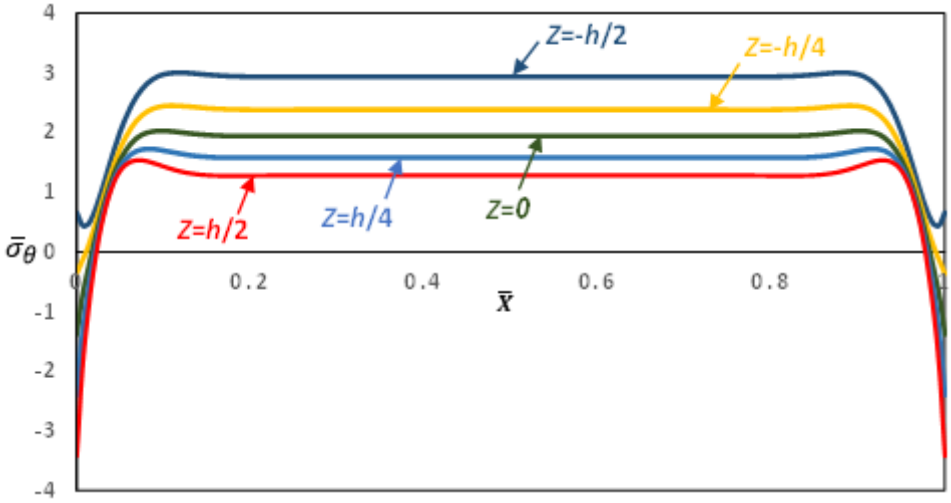


Fig. 5. Distribution of circumferential stress along the surfaces

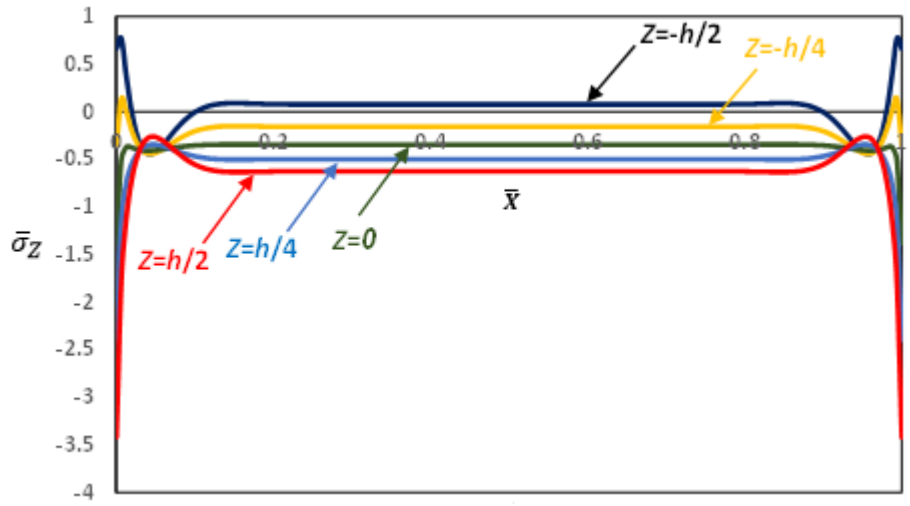


Fig. 6. Radial stress distribution along the surfaces

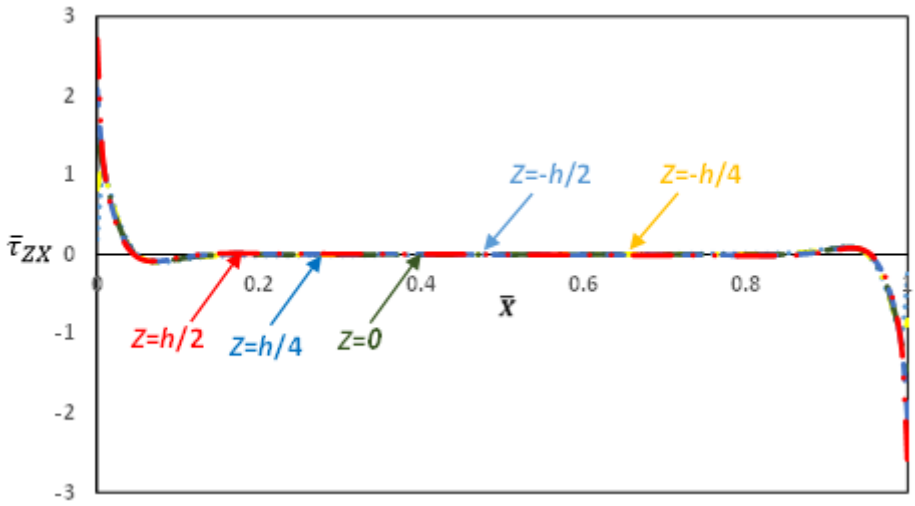


Fig. 7. Distribution of shear stress along the surfaces

As shown in Fig. 7, the critical values of the shear stress occurred in the border areas of the cylindrical shell, and the stress value in the regions far from the borders is independent of the layers of the cylindrical shell.

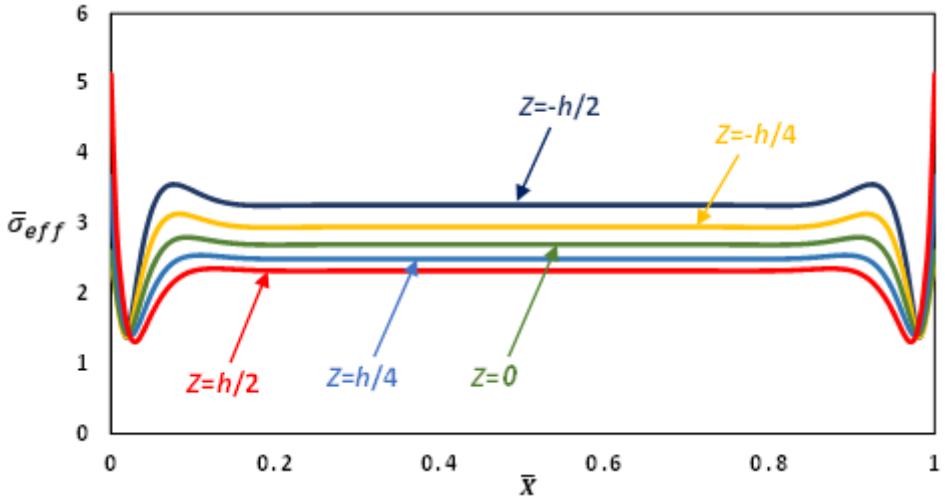
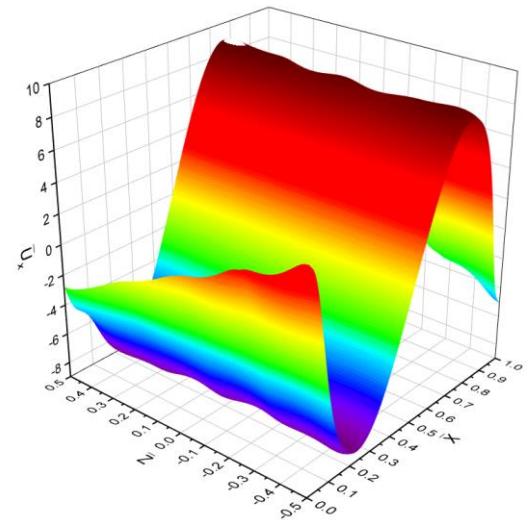
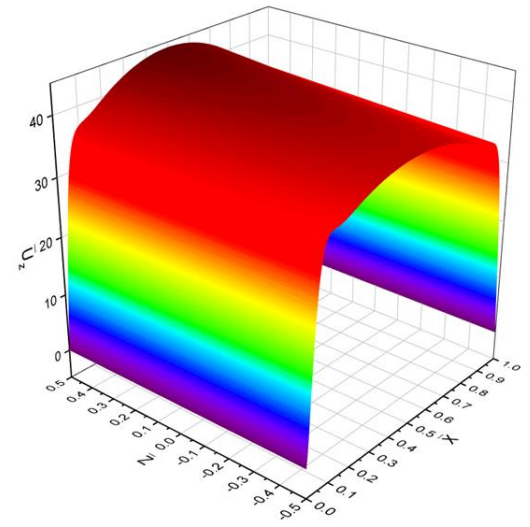


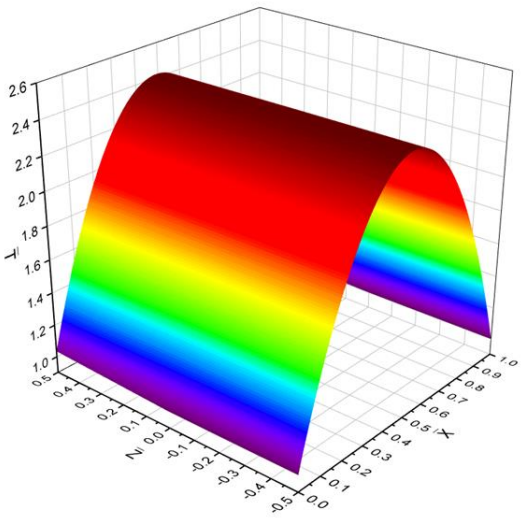
Fig. 8. Von Mises stress distribution along surfaces



(a)



(b)



(c)

Fig. 9. Distribution of non-dimensional axial (a) and radial (b) displacement and temperature (c) in the cylinder

The distribution of circumferential stress and von Mises stress is presented in Fig. 8. It can be seen that the circumferential and von Mises stresses of the cylindrical shell under the influence of mechanical and thermal loading have maximum values in the border regions and constant values in the middle areas.

4.2. Clamped-Free boundary condition

In the second case, the cylindrical shell is subjected to mechanical and thermal loading under fixed mechanical boundary conditions and a temperature $T = 25℃$, and the other end is considered to be mechanically free and thermally insulated. In Figs.10 to 12, the effects of boundary conditions on mechanical and thermal behaviors in temperature distribution and radial and axial displacements for different heights and levels of the cylinder have been investigated.

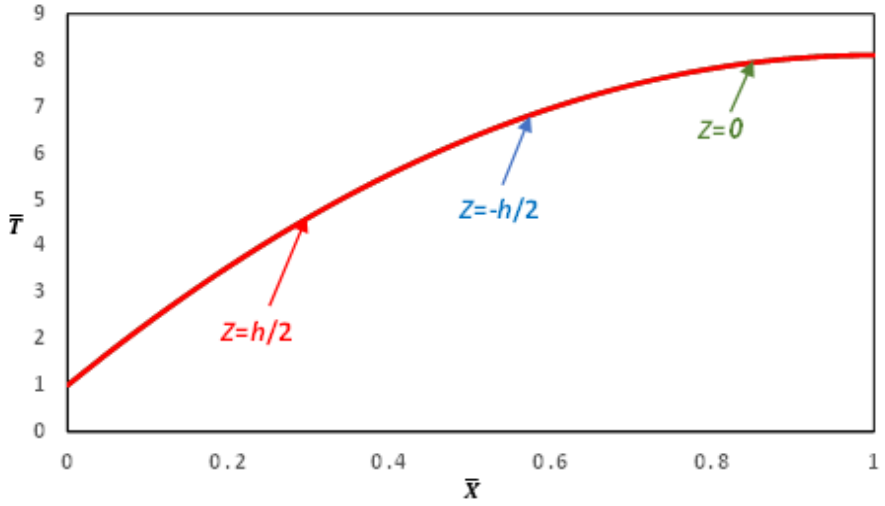


Fig. 10. Temperature distribution along the cylindrical shell

The change of the boundary conditions shows that the maximum values of temperature and displacements are much higher than in the first case and occur at the insulated and free ends of the cylinder.

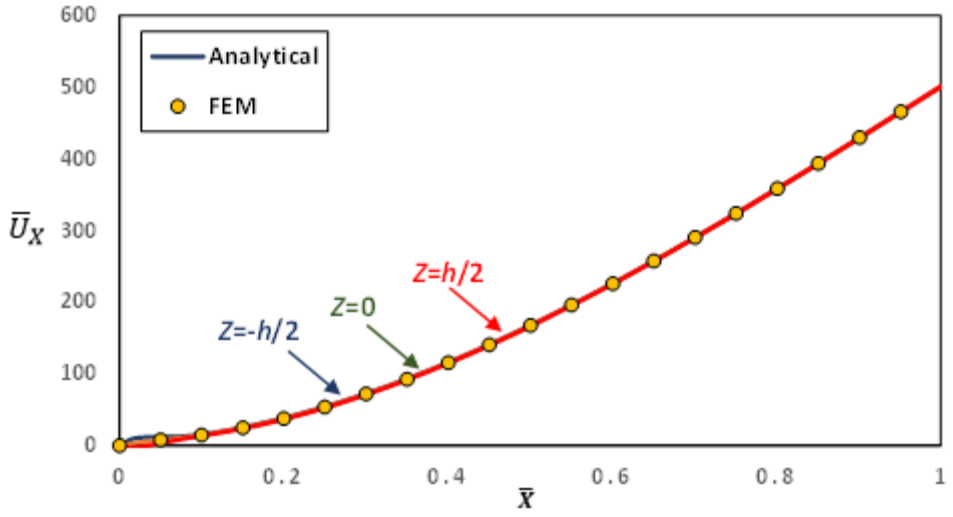


Fig. 11. Axial displacement distribution along the cylindrical shell

In the second case, the maximum temperature and radial displacement (Figs. 10 and 12) are almost three times higher than the values of the first case. According to Fig. 11, the maximum axial displacement is 60 times greater than the value of the first case. Also, in the second case, the axial displacement profile is independent of the radial direction and changes along the axial direction with the boundary conditions change. The axial displacement is somewhat independent of the radial direction and varies primarily along the axial direction.

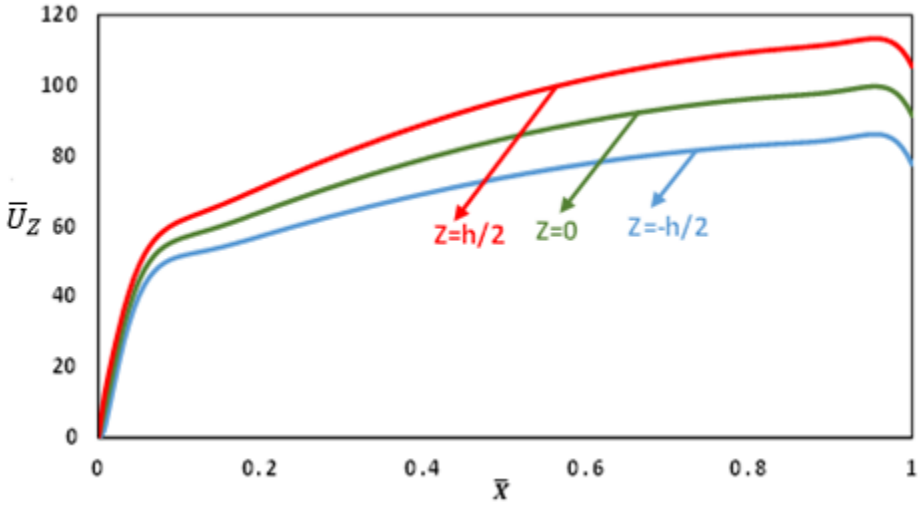


Fig. 12. Radial displacement distribution along the cylindrical shell

The investigation of circumferential, radial, shear, and effective stresses in different layers of the cylinder is done in Figs. 13-16. The Distribution of axial and radial displacements, and temperature in different layers of the thickness and length of the cylinder is done in Fig. 17. The change in the cylindrical shell's boundary conditions shows that the circumferential and von Mises stresses decrease as one moves away from the inner layer and mechanical and thermal loading. Also, these stresses are constant in the areas away from the boundaries, and the maximum values occur around the boundaries.

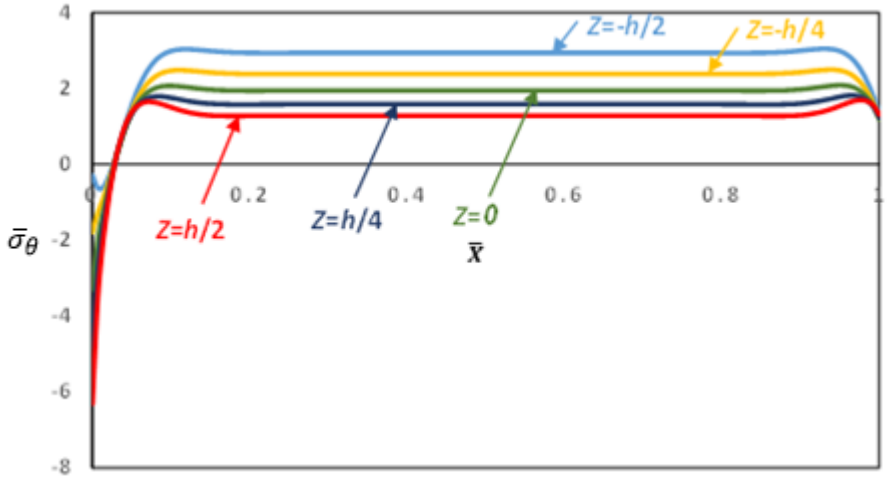


Fig. 13. Distribution of circumferential stress along the surfaces

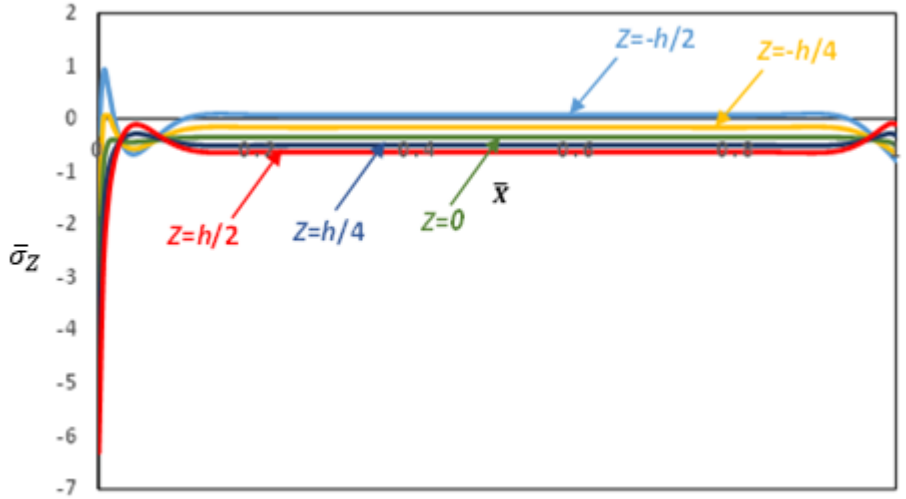


Fig. 14. Radial stress distribution along the surfaces

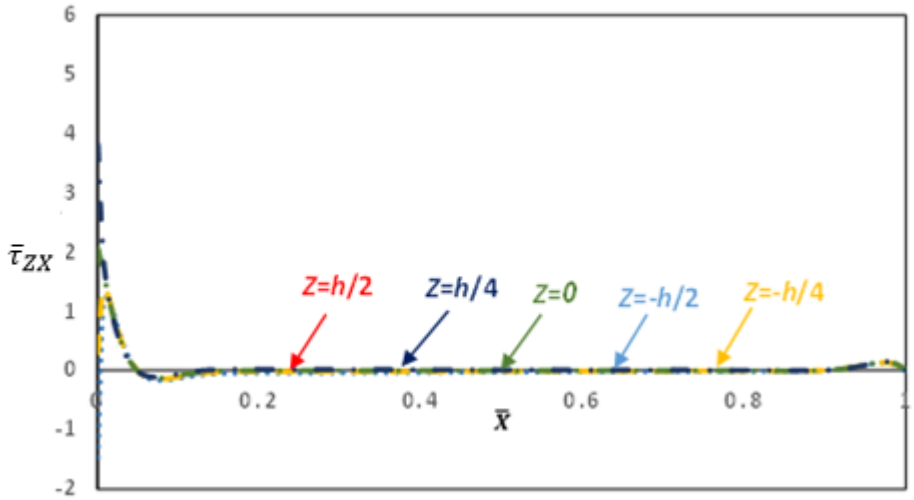


Fig. 15. Distribution of shear stress along the surfaces

As shown in Fig. 15, the critical values of the shear stress occurred in the border areas of the cylindrical shell, and the stress value in the regions far from the borders is independent of the layers of the cylindrical shell.

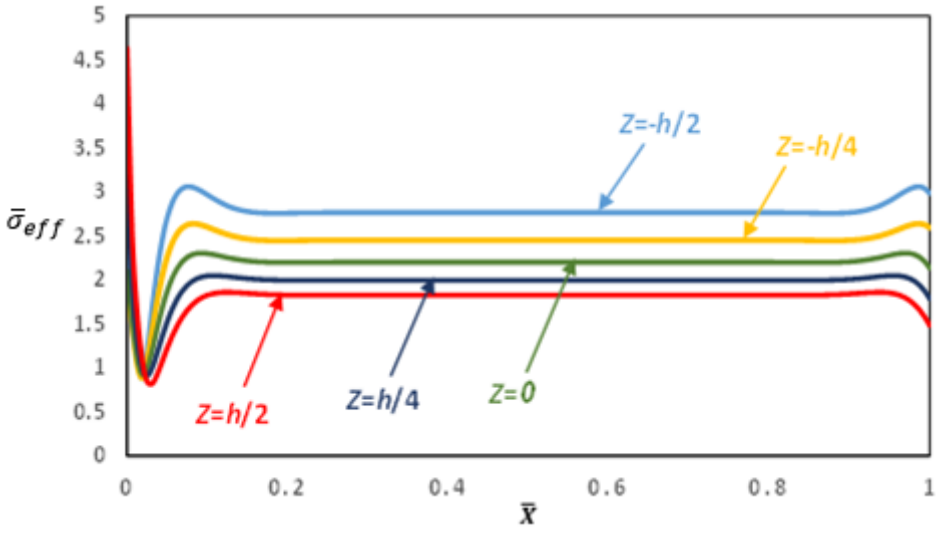


Fig. 16. Von Mises stress distribution along surfaces

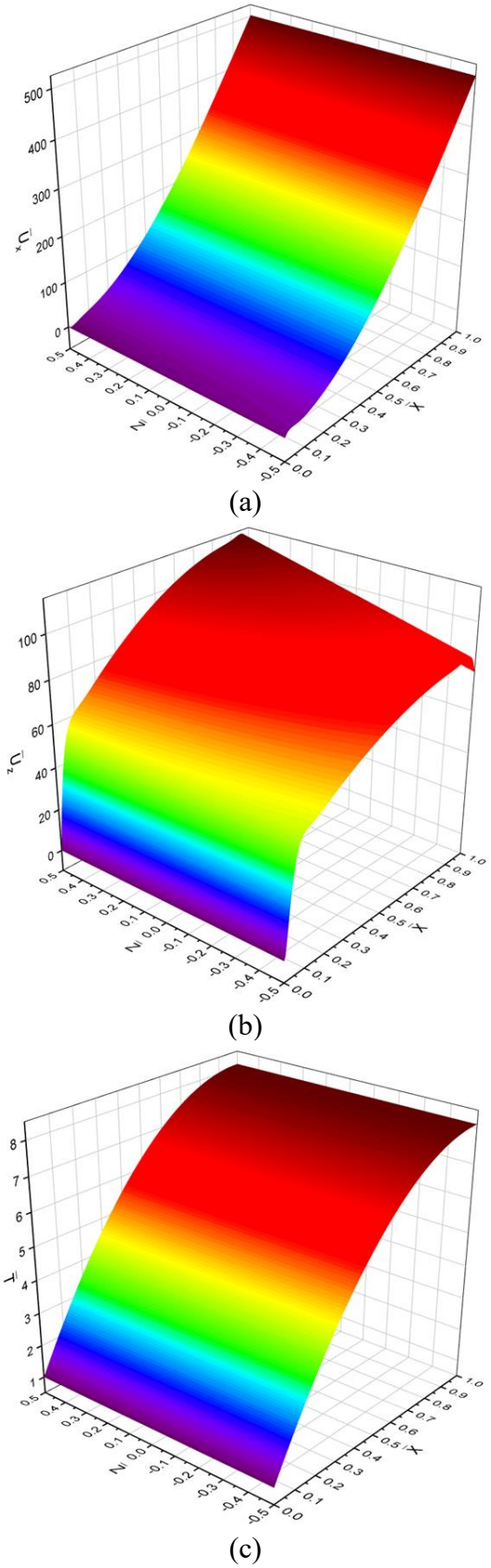


Fig. 17. Distribution of non-dimensional axial (a) and radial (b) displacement and temperature (c) in the cylinder

The data obtained from the analytical solution and finite element simulation are presented in Table 1.

Table.1. Numerical comparison of analytical data and FEM

Clamped-clamped & temperature-temperature ends						
Surface	**Method**	T(℃)	$U_z(mm)$	$U_x(mm)$	$\sigma_{eff}(MPa)$	$\sigma_\theta(MPa)$
Middle	MAM	60.6269	0.0787	0	261	240
	FEM	60.6269	0.0799	0	268	230
Inner	MAM	60.5252	0.0835	0	216	156
	FEM	60.6269	0.0836	0	216	130
Clamped-free & temperature-insulated ends						
Surface	**Method**	T(℃)	$U_z(mm)$	$U_x(mm)$	$\sigma_{eff}(MPa)$	$\sigma_\theta(MPa)$
Middle	MAM	158.3847	0.1129	0. 360	257	240
	FEM	158.21	0.11	0. 365	256	232
Inner	MAM	158.3365	0.17	0. 355	216	160
	FEM	158.15	0.1681	0. 358	211	156

The above table compares the results of matched asymptotic method (MAM) solution and the finite element in the inner and middle layers of the cylindrical shell. It can be seen that in two cases, the matched asymptotic method (MAM) solution is in good agreement with the finite element solution. The obtained results show that in the first case, the values and displacements of the cylindrical shell temperature are much lower than in the case where the end of the cylindrical shell is free and insulated.

5. Conclusions

The paper provides an exact analytical solution for an axisymmetric thick-walled cylindrical shell subjected to pressure and thermal loading, accommodating arbitrary boundary conditions. Initially, the governing equilibrium equations were derived utilizing the energy method, the first-order shear deformation theory, and the first-order temperature theory. Subsequently, the extracted equations were transformed into a set of differential equations with constant coefficients by using the analytical method of the matched asymptotic expansion of the perturbations technique, and the values of displacements and temperature parameters were ascertained by summing the external solution and solving the set of equations at the boundaries. Ultimately, the results obtained are categorized as follows:

- The application of first-order temperature theory in this study enables the inclusion of temperature parameters as unknowns within the system's governing equations. This facilitates the resolution and simulation of similar problems under varying boundary conditions and the capability to address the problem across diverse states.
- A comparison between the current findings (based on two-dimensional thermal analysis) and existing literature (utilizing one-dimensional thermal analysis) reveals a strong dependence of temperature fields on the axial direction of the cylinder, even in regions far from both ends.
- Comparing the outcomes of applying matched asymptotic method (MAM) of the perturbations technique to solve a problem with those obtained by addressing it as an eigenvalue problem (EVP) reveals a closer and more precise match with the finite element method's solution.
- This analytical method is highly appropriate for examining the impact of mechanical and thermal conditions at both ends of a cylinder. The results have indicated significant alterations in stress patterns, particularly shear and circumferential stress, occur near its two ends. It is essential to consider the safety factor when designing these cylinders.
- The results indicate that under identical loading conditions, the mechanical and thermal behavior of the shell experiences substantial alterations when the boundary conditions are modified.

References

[1] Ghannad M., Nejad M.Z., Rahimi G.H. (2009): Elastic solution of axisymmetric thick truncated conical shells based on first-order shear deformation theory, Mechanika, Vol. 79, No. 5, pp. 13-20.

[2] Ghannad M., Nejad M.Z. (2010): Elastic analysis of pressurized thick hollow cylindrical shells with clamped-clamped ends, Mechanika, Vol. 85, No. 5, pp. 11-18.

[3] Ghannad M., Nejad M.Z. (2012): Elastic analysis of heterogeneous thick cylinders subjected to internal or external pressure using shear deformation theory, Acta Polytechnica Hungarica, Vol. 9, No. 6, pp. 117-136. https://doi.org/ 10.12700/APH.9.6.2012.6.8

[4] Ghannad M., Rahimi G.H., Nejad M.Z. (2013): Elastic analysis of pressurized thick cylindrical shells with variable thickness made of functionally graded materials, Composites Part B: Engineering, Vol. 45, No. 1, pp. 388-396. https://doi.org/10.1016/j.compositesb.2012.09.043

[5] Shojaeefard M.H., Najibi A. (2014): Nonlinear transient heat conduction analysis of hollow thick temperature-dependent 2D-FGM cylinders with finite length using numerical method, Journal of Mechanical Science and Technology, Vol. 28, No. 8, pp. 3825-3835. https://doi.org/ 10.1007/s13369-014-1403-1

[6] Jiang H., Dai H. (2015): Analytical solution for three-dimensional steady and transient heat conduction problems of a double-layer plate with a local heat source, International Journal of Heat and Mass Transfer, Vol. 89, pp. 652-666. https://doi.org/10.1016/j.ijheatmasstransfer.2015.05.094

[7] Ghannad M., Parhizkar Yaghoubi M. (2015): A thermoelasticity solution for thick cylinders subjected to thermo-mechanical loads under various boundary conditions, International Journal Advanced Design and Manufacturing Technology, Vol. 8, No. 4, pp. 1-12.

[8] Jabbari M., Nejad M.Z., Ghannad M. (2015): Thermo-elastic analysis of axially functionally graded rotating thick cylindrical pressure vessels with variable thickness under mechanical loading, International Journal of Engineering Science, Vol. 96, pp. 1-18. https://doi.org/10.1016/j.ijengsci.2015.07.005

[9] Khoshgoftar M.J., Mirzaali M.J., Rahimi G.H. (2015): Thermoelastic analysis of non-uniform pressurized functionally graded cylinder with variable thickness using first order shear deformation theory (FSDT) and perturbation method, Chinese Journal of Mechanical Engineering, Vol. 28, No. 6, pp. 1149-1158. https://doi.org/ 10.3901/CJME.2015.0429.048

[10] Arefi M., Koohi Faegh R., Loghman A. (2016): The effect of axially variable thermal and mechanical loads on the 2D thermoelastic response of FG cylindrical shell, Journal of Thermal Stresses, Vol. 39, No. 12, pp. 1-21. http://dx.doi.org/10.1080/01495739.2016.1217178

[11] Ghannad M., Parhizkar Yaghoobi M. (2017): 2D thermo elastic behavior of a FG cylinder under thermomechanical loads using a first order temperature theory, International Journal of Pressure Vessels and Piping, Vol. 149, pp. 75-92. https://doi.org/ 10.1016/j.ijpvp.2016.12.002

[12] Vaziri A., Ghannad M., Anwar Bég O. (2018): Exact thermoelastic analysis of thick cylindrical functionally graded material shell under unsteady heating using first order shear deformation theory, Heat Transfer-Asian Research, Vol. 48, No. 5, pp. 1737-1760. https://doi.org/10.1002/htj.21455

[13] Mehditabar A., Rahimi G.H., Malekzadeh Fard K. (2018): Thermoelastic analysis of rotating functionally graded truncated conical shell by the methods of polynomial based

differential quadrature and fourier expansion-based differential quadrature, Mathematical Problems in Engineering, Vol. 2018, pp. 1-18. https://doi.org/10.1155/2018/2804123

[14] Arefi M., Mohammadi M., Tabatabaeian A., Dimitri R., Tornabene F. (2018): Two-dimensional thermo-elastic analysis of FG-CNTRC cylindrical pressure vessels, Steel and Composite Structures, Vol. 27, No. 4, pp. 525-536. https://doi.org/10.12989/scs.2018.27.4.525

[15] Gharooni H., Ghannad M. (2019): Nonlinear analysis of radially functionally graded hyperelastic cylindrical shells with axially-varying thickness and non-uniform pressure loads based on perturbation theory, Journal of Computational Applied Mechanics, Vol. 50, No. 2, pp. 324-340. https://doi.org/ 10.22059/JCAMECH.2019.282149.401

[16] Parhizkar Yaghoubi M., Ghannad M. (2020): An analytical solution for temperature distribution and thermal strain of FGM cylinders with varying thickness and temperature-dependent properties using perturbation technique, Journal of Computational Applied Mechanics, Vol. 51, No. 1, pp. 144-156. https://doi.org/ 10.22059/JCAMECH.2020.294821.464

[17] Omidi Bidgoli M., Loghman A., Arefi M., Koohi R. (2020): Transient stress and deformation analysis of a shear deformable FG rotating cylindrical shell made of AL-SIC subjected to thermo-mechanical loading, Australian Journal of Mechanical Engineering, Vol. 21, No. 1, pp. 279-294. https://doi.org/10.1080/14484846.2020.1842296

[18] Benslimane A., Benchallal R., Mammeri S., Methia M., Khadimallah M.A. (2020): Investigation of displacements and stresses in thick-walled FGM cylinder subjected to thermo-mechanical loadings, International Journal for Computational Methods in Engineering Science and Mechanics, Vol. 22, No. 2, pp. 138-149. https://doi.org/10.1080/15502287.2020.1853853

[19] Najibi A., Alizadeh P., Ghazifard P. (2020): transient thermal stress analysis for a short thick hollow FGM nonlinear temperature-dependent material properties, Journal of Thermal Analysis and Calorimetry, Vol. 146, pp. 1971-1982. https://doi.org/ 10.1007/s10973-020-10442-2

[20] Eliasi H., Bateni M., Eslami M.R. (2021): Coupled thermoelasticity of FGM truncated conical shells, Iranian Journal of Mechanical Engineering Transactions of the ISME, Vol. 22, No. 1, pp. 127-142. https://doi.org/ 10.30506/JMEE.2021.132091.1240

[21] Salehi A., Ahmadi I. (2022): Transient thermal and mechanical stress analysis of 2d-functionally graded finite cylinder:A truly meshless formulation: Iranian Journal of Science and Technology, Transactions of Mechanical Engineering, Vol. 46, pp. 573-598. https://doi.org/ 10.1007/s40997-021-00432-6

[22] Tokovyy Yuriy V. (2024): Elastic and thermoelastic response of multilayer inhomogeneous hollow cylinders, Mechanics of Advanced Materials and Structures, Vol. 31, No. 17, pp. 3889-3901. https://doi.org/10.1080/15376494.2023.2186548

[23] Avey M., Fantuzzi N., Sofiyev A.H. (2023): Thermoelastic stability of CNT patterned conical shells under thermal loading in the framework of shear deformation theory, Mechanics of Advanced Materials and Structures, Vol. 30, No. 9, pp. 1828-1841. https://doi.org/10.1080/15376494.2022.2045653

[24] Ramezani F., Nejad M.Z., Ghannad M. (2023): Thermoelastic analysis of rotating thick-walled cylindrical pressure vessels with linear variable thickness under bi-directional temperature, Journal of Computational Applied Mechanics, Vol. 54. No. 4, pp. 515-532. https://doi.org/ 10.22059/JCAMECH.2023.365220.876

[25] Ghadimi M., Ghannad M. (2024): Elasto-plastic stress analysis of thick walled cylinders using shear deformation theories and radial return method, Iranian Journal of Mechanical

Engineering Transactions of the ISME, Vol. 25, No. 2, pp. 1-14. https://doi.org/10.30506/JMEE.2024.2023842.1342

[26] Sofiyev A.H., Avey M. (2025): Laminated Nanocomposite structural elements in thermal environments: Mathematical modeling and applications, Mathematical Methods in the Applied Sciences, 17 pages. https://doi.org/10.1002/mma.10820

[27] Witt F.J. (1965): Thermal analysis of cylindrical shells, Nuclear Structural Engineering, Vol. 1, No. 3, pp. 276-284. https://doi.org/10.1016/0369-5816(65)90111-0

[28] Tzou H.S., Bao Y. (1995): A theory on anisotropic piezothermoelastic shell laminates with sensor/actuator applications, Journal of Sound and Vibration, Vol. 184, No. 3, pp. 453-473. https://doi.org/10.1006/jsvi.1995.0328

[29] Mahboubi Nasrekani F., Eipakchi H.R. (2014): Nonlinear analysis of cylindrical shells with varying thickness and moderately large deformation under nonuniform compressive pressure using the first order shear deformation theory, Journal of Engineering Mechanics, Vol. 141, No. 5, pp. 04014153(1-11). https://doi.org/10.1061/(ASCE)EM.1943-7889.0000875

[30] Nayfeh A.H. (2011): Introduction to Perturbation Techniques, John Wiley, New York.

Appendix

The extracted non-zero coefficients matrix is as follows:

K is the shear correction factor embedded in the shear stress expression. It is assumed that in the static state, for cylindrical shells $K = 5/6$.

$$A_{11} = \int_{-\frac{h}{2}}^{\frac{h}{2}} (1-\nu)(R+z)dz,\ A_{12} = \int_{-\frac{h}{2}}^{\frac{h}{2}} (1-\nu)(R+z)zdz,\ A_{21} = -\int_{-\frac{h}{2}}^{\frac{h}{2}} (1-\nu)(R+z)zdz$$

$$A_{22} = -\int_{-\frac{h}{2}}^{\frac{h}{2}} (1-\nu)(R+z)z^2dz,\ \ A_{33} = -\int_{-\frac{h}{2}}^{\frac{h}{2}} \frac{K}{2}(1-2\nu)(R+z)dz$$

$$A_{34} = -\int_{-\frac{h}{2}}^{\frac{h}{2}} \frac{K}{2}(1-2\nu)(R+z)zdz,\ \ A_{43} = -\int_{-\frac{h}{2}}^{\frac{h}{2}} \frac{K}{2}(1-2\nu)(R+z)z^2dz$$

$$A_{55} = -\int_{-\frac{h}{2}}^{\frac{h}{2}} \frac{K}{R}(1+\nu)(1-2\nu)(R+z)dz,\ \ A_{56} = -\int_{-\frac{h}{2}}^{\frac{h}{2}} \frac{K}{R}(1+\nu)(1-2\nu)(R+z)zdz$$

$$A_{65} = -\int_{-\frac{h}{2}}^{\frac{h}{2}} K(1+\nu)(1-2\nu)(R+z)zdz,\ \ A_{65} = -\int_{-\frac{h}{2}}^{\frac{h}{2}} K(1+\nu)(1-2\nu)(R+z)z^2dz$$

$$B_{13} = \int_{-\frac{h}{2}}^{\frac{h}{2}} \nu dz, B_{14} = \int_{-\frac{h}{2}}^{\frac{h}{2}} \nu(R+2z)dz,\ B_{15} = -\int_{-\frac{h}{2}}^{\frac{h}{2}} \alpha(1+\nu)(R+z)dz$$

$$B_{16} = -\int_{-\frac{h}{2}}^{\frac{h}{2}} \alpha(1+\nu)(R+z)zdz,\ \ B_{23} = -\int_{-\frac{h}{2}}^{\frac{h}{2}} \nu zdz + \int_{-\frac{h}{2}}^{\frac{h}{2}} \frac{K}{2}(1-2\nu)(R+z)dz$$

$$B_{24} = -\int_{-\frac{h}{2}}^{\frac{h}{2}} \nu z^2dz + \int_{-\frac{h}{2}}^{\frac{h}{2}} \frac{K}{2}(1-2\nu)(R+z)zdz - \int_{-\frac{h}{2}}^{\frac{h}{2}} \nu(1-2\nu)(R+z)zdz$$

$$B_{25}=-\int_{-\frac{h}{2}}^{\frac{h}{2}}\alpha(1+\nu)(R+z)zdz,\ \ B_{26}=-\int_{-\frac{h}{2}}^{\frac{h}{2}}\alpha(1+\nu)(R+z)z^2dz, B_{31}=\int_{-\frac{h}{2}}^{\frac{h}{2}}\nu dz$$

$$B_{32}=-\int_{-\frac{h}{2}}^{\frac{h}{2}}\nu z dz-\int_{-\frac{h}{2}}^{\frac{h}{2}}\frac{K}{2}(1-2\nu)(R+z)dz,\ \ B_{416}=-\int_{-\frac{h}{2}}^{\frac{h}{2}}\nu z dz+\int_{-\frac{h}{2}}^{\frac{h}{2}}\nu(R+z)dz$$

$$B_{42}=-\int_{-\frac{h}{2}}^{\frac{h}{2}}\nu z^2dz+\int_{-\frac{h}{2}}^{\frac{h}{2}}\nu(R+z)zdz-\int_{-\frac{h}{2}}^{\frac{h}{2}}K(1-2\nu)(R+z)zdz$$

$$C_{22}=-\int_{-\frac{h}{2}}^{\frac{h}{2}}\frac{K}{2}(1-2\nu)(R+z)dz\,, C_{33}=-\int_{-\frac{h}{2}}^{\frac{h}{2}}\frac{(1-\nu)}{(R+z)}dz\,, C_{34}=\int_{-\frac{h}{2}}^{\frac{h}{2}}\frac{(1-\nu)}{(R+z)}zdz+\int_{-\frac{h}{2}}^{\frac{h}{2}}\nu dz$$

$$C_{35}=-\int_{-\frac{h}{2}}^{\frac{h}{2}}\alpha(1+\nu)dz\,,\ C_{36}=-\int_{-\frac{h}{2}}^{\frac{h}{2}}\alpha(1+\nu)zdz\,,\ C_{43}=\int_{-\frac{h}{2}}^{\frac{h}{2}}\frac{(1-\nu)}{(R+z)}zdz+\int_{-\frac{h}{2}}^{\frac{h}{2}}\nu dz$$

$$C_{44}=\int_{-\frac{h}{2}}^{\frac{h}{2}}\frac{(1-\nu)}{(R+z)}z^2dz+2\int_{-\frac{h}{2}}^{\frac{h}{2}}\nu dz+\int_{-\frac{h}{2}}^{\frac{h}{2}}(1+\nu)(R+z)dz$$

$$C_{45}=\int_{-\frac{h}{2}}^{\frac{h}{2}}-\alpha(1+\nu)zdz-\int_{-\frac{h}{2}}^{\frac{h}{2}}\alpha(1+\nu)(R+z)dz$$

$$C_{54}=\int_{-\frac{h}{2}}^{\frac{h}{2}}-\alpha(1+\nu)z^2dz-\int_{-\frac{h}{2}}^{\frac{h}{2}}\alpha(1+\nu)(R+z)zdz,\ \ C_{66}=-\int_{-\frac{h}{2}}^{\frac{h}{2}}K(R+z)dz$$

$$D_{2i_{15}}=-R^*h^*(1+\nu), D_{2i_{24}}=-\frac{1}{12}R^*h^{*3}(1-\nu), D_{2i_{31}}=-\mu R^*h^*, D_{2i_{32}}=-\frac{1}{12}\mu h^{*3}$$

$$D_{2i_{35}}=-h^*(1+\nu),\ D_{2i_{41}}=-\tfrac{1}{12}\mu h^{*3}, D_{2i_{35}}=-R^*h^*(1+\nu),\ D_{2i_{32}}=-\tfrac{1}{12}KR^*h^{*3}$$

$$D_{1i_{14}}=-\tfrac{1}{12}h^{*3}(1-\nu),\ D_{1i_{21}}=\mu R^*h^*,\ D_{1i_{22}}=\tfrac{1}{12}(\mu-2\nu)h^{*3},\ D_{1i_{23}}=-\tfrac{1}{12}(1-\nu)h^{*3}$$

$$D_{1i_{26}}=\tfrac{1}{12}R^*h^{*3}(1+\nu),\ D_{1i_{34}}=-\mu R^*h^*,\ D_{1i_{44}}=-\tfrac{1}{12}(\mu-2\nu)h^{*3},\ D_{1i_{56}}=-\tfrac{1}{12}\tfrac{K^*h^{*3}}{R^*}$$

$$D_{1i_{65}}=-\frac{1}{12}K^*h^{*3},\ D_{0i_{11}}=\nu h^*, D_{0i_{12}}=\nu R^*h^*,\ D_{0i_{13}}=R^*h^*(1-\nu)$$

$$D_{0i_{16}}=-\tfrac{1}{12}h^*(1+\nu),\ D_{0i_{24}}=\mu R^*h^*, D_{0i_{25}}=\tfrac{1}{12}h^{*3}(1+\nu),\ D_{0i_{31}}=\beta(1-\nu),$$

$$D_{0i_{32}}=h^*-R^*\beta(1-\nu),\ D_{0i_{53}}=\nu h^*,\ D_{0i_{41}}=h^*-R^*\beta(1-\nu),\ D_{0i_{42}}=R^{*2}\beta(1-\nu)$$

$$D_{0i_{43}}=\nu R^*h^*,\ D_{0i_{46}}=-\tfrac{1}{6}h^{*3}(1+\nu),\ D_{0i_{55}}=-K^*h^*,\ D_{0i_{66}}=-K^*R^*h^*$$